Proceedings of the ICBBG2025
2025 International conference on Bio-mediated and Bio-inspired Geotechnics
18-20 May, 2025 | Tempe, Arizona, USA
https://doi.org/10.53243/ICBBG2025-105

Microscopic Insights into MICP Treated Fly Ash

Shaivan. H. Shivaprakash[1] and Susan. E. Burns[2]

[1]* School of Civil and Environmental Engineering, Georgia Institute of Technology, 790 Atlantic Drive, Atlanta, GA 30332, United States. Email: shaivan.hs@gatech.edu. Corresponding Author

[2]School of Civil and Environmental Engineering, Georgia Institute of Technology, 790 Atlantic Drive, Atlanta, GA 30332, United States. Email: sburns@gatech.edu

ABSTRACT

Historically, the byproducts of coal combustion are either used beneficially in products (e.g., concrete, wallboard) or are land disposed in ponded storage facilities or landfills. However, long term storage of ponded ash can result in mechanical stability issues or in leaching into groundwater, making the precipitation of a binding matrix desirable from both a geotechnical and environmental perspective. The present study provides microscopic insights into the applicability and effect of using microbially induced calcite precipitation (MICP) on fly ash. MICP column experiments were performed on a loosely packed fly ash material and bio-cemented samples were preserved for SEM imaging. SEM observations showed the presence of microbial cells, with some cells growing to roughly the same scale as the smallest fly ash spheres. The presence of microbial colonies in the bio-cemented fly ash samples indicated that biological activity was occurring in fly ash. The precipitated calcite crystals formed a cementation matrix in which the fly ash particles were embedded rather than forming particle-to-particle cementation bonds between individual fly ash particles owing to the small size of tested fly ash particles, and resulted in larger aggregated units of cemented fly ash particles.
Keywords: Fly Ash, Bacteria, Cementation matrix, Aggregation

INTODUCTION

Fly ash is a lightweight residual material produced from the combustion of coal and other fuel sources for electricity generation. Although ~60% of fly ash and other coal combustion products (CCPs) produced are beneficially used in a range of applications from cement and concrete to geotechnical applications to gypsum wall board (Adams 2022)), the residual fly ash is land disposed. In 2022, roughly 11 million short tons of fly ash were disposed in ponds and landfills, and it is estimated that there are over 1,400 ponds and landfills across the US containing stored legacy ash (Black 2015).

Fly ash is generally wet disposed into ponds through sluicing; however, this technique results in a low-density fill as the lightweight fly ash particles remain suspended in water. Such ponds are less mechanically stable and are prone to failure triggering mechanisms such as heavy rains, flooding, internal piping erosion, and other natural hazard events. The 2008 Kingston pond failure resulted in the release of ~5.4 million cubic yards of coal ash in Tennessee and ~50,000-82,000 tons of coal ash were released in North Carolina in the Dan River coal ash spill, which caused significant economic losses and environmental damage. Furthermore, leaching of coal ash

into groundwater is also a potential problem. Therefore, stabilization techniques to improve the stability and safety of fly ash ponds are necessary to prevent such failures.

Microbially induced calcite precipitation (MICP) is an emerging ground improvement technique that shows promising sustainability metrics and has been proposed for applications like soil stabilization, liquefaction mitigation, dust suppression, groundwater remediation, sealing of fractures, and concrete remediation ((Achal et al. 2011; Choi et al. 2017; Chu et al. 2012; Cuthbert et al. 2013; DeJong et al. 2022; Feng et al. 2021; Kang et al. 2014; Montoya et al. 2013; Phillips et al. 2013, 2016)). Montoya et al. (2019) and Safavizadeh et al. (2019) have explored the beneficial use of coal ash using MICP and obtained mixed results, with successful application of MICP in two out of three ash samples. The changes in macroscale properties (hydraulic conductivity, compressibility, and shea-wave velocity) of MICP treated ash samples are well documented (Montoya et al. 2019; Safavizadeh et al. 2019); however, the microscopic insights into MICP treated ash are still lacking in literature.

The objective of the present study is to evaluate the efficacy of MICP in a low-density material like fly ash, and investigate the presence and association of microbial cells on fly ash particles, impact of fly ash morphology and chemistry on precipitated calcite and formation of cementation bonds. MICP column experiments were performed on an unweathered class F fly ash sample, and bio-cemented specimens were preserved for scanning electron microscopy for microstructural analysis.

MATERIALS AND METHODS

Fly Ash Sample.

An unweathered Class F fly ash produced in a large coal combustion plant in the southeastern U.S. was used for MICP column experiments. Additional details on the characterization of the samples can be found in (Wirth et al. 2019b; a). An Ottawa F-110 sand sample was used as the benchmark material to compare MICP performance in fly ash.

Particle Size Distribution.

Malvern Panalytical Mastersizer 3000E was used to determine the particle size of untreated and MICP fly ash samples. The intensity of light scattering was measured and the data was analyzed using the Malvern Panalytical software to determine the size fraction of particles. Fly ash samples of <5g were suspended in a beaker of 600 mL of distilled water, and particles were wet dispersed using Hydro EV configuration of Mastersizer along with sonication.

MICP Bio-stimulation Treatment of Fly Ash.

The MICP experimental setup consisted of cylindrical stainless steel test columns (3 in. diameter and 6 in. height) with top and bottom Teflon end caps (Figure 1). Plastic polyester filters (75 μm) were used at the inlet and outlet of the cylinder to minimize loss of fly ash. The components of the experimental apparatus (e.g., tubing, pipe fittings, and column) were acid-washed to remove salts and precipitates, and subsequently washed with deionized water and ethanol to minimize residual microbial activity. The fly ash sample was placed in the column by wet deposition, achieving a dry density of 0.8 g/cm^3 (dry density of 1.73 g/cm^3 achieved for Ottawa F-110 sand sample), which was low due to the low specific gravity and the hydrophobicity of the fly ash particles. A bottom-up flow treatment scheme with a low flow rate of 4 mL/min (15 mL/min for Ottawa F-110 sample), was adopted to minimize flushing of fine particles, air entry, and to ensure saturation of the sample. To prevent piping failure in the soil column due to high pumping rates, a vertical stress of 100 kPa

was applied to the top cap using a spring system. Silicone caulking and epoxy resin were applied externally on the connections and fittings to minimize leakage.

Figure 1. MICP experimental column setup used in the present study.

MICP biostimulation treatment in which the native ureolytic microbes are stimulated to perform urea hydrolysis was adopted. This treatment scheme consisted of initially flushing the column with urea-rich bio-stimulation solutions followed by injection of cementation solutions. Treatment solutions of 500 ml volume were used (chemical formulations are provided in Table 1). After the 1st stimulation treatment, a period of 48 hours was allowed for the growth and development of ureolytic microbial community (Gomez et al. 2018; Lee et al. 2019), after which three additional stimulation treatments were performed at 24-hour intervals. Before the start of cementation treatment phase, a flush treatment solution was injected to prevent abiotic calcite precipitation. Cementation treatments were provided every 24 hours for a period of 10 days, after which the columns were disassembled, and samples were preserved with biological treatment for SEM imaging.

Table 1. Concentration of Chemical Constituents for Each Treatment Formulation.

Chemical constituent	Treatment		
	Stimulation	Flush	Cementation
Urea (mM)	350	-	250
Ammonium chloride (mM)	100	12.5	12.5
Sodium acetate trihydrate (mM)	42.5	42.5	42.5
Yeast extract (g/L)	2.0	2.0	2.0
Calcium chloride (mM)	-	-	250
pH	9	-	-

Scanning Electron Microscopy.

Field Emission - Scanning electron microscopy (FE-SEM) was performed under low voltage conditions of 3 kV (Hitachi SU8230). Specimens were coated with palladium and gold to a thickness of 15-20 nm (Quorum Q150V Plus) to reduce charging. Scanning electron microscopy

- Energy Dispersive X-ray Spectroscopy (SEM-EDS) was performed on the same instrument with an Oxford EDS detector. The Aztec software suite was used to record and analyze the EDS data. EDS maps were performed at 1024x768 resolution, 5 frames per map, pixel dwell time of 50 µs, and process time constant between 4 and 5 to obtain sufficient counts and detector dead time for EDS analysis.

Biological sample preparation for SEM was done to obtain SEM images of bacterial cells grown on fly ash particles during the MICP process. After the final cementation treatment, the column was disassembled, and small cemented fly ash samples were carefully immersed in a fixating agent (glutaraldehyde 2%, paraformaldehyde 2% in phosphate buffer of pH 7.4) to stabilize and prevent the biological structures from decomposition. The sample was immersed in the fixation agent for 1 hour in a fume hood and then moved to 4° C in the refrigerator. After 24 hours, the excess fixation agent was removed by rinsing with deionized water and the sample was immersed in phosphate-buffered saline (PBS). It was then immersed in deionized water to dissolve any remaining salts, followed by drying with ethanol in sequential concentrations of 20%, 35%, 50%, 75%, 90%, and 100% for 30 minutes each. This was followed by a final drying step using Hexamethyldisilazane (HMDS). Finally, the specimen was sputter coated for SEM imaging.

Chemical Measurements.

The quantity of carbonate minerals in the soil sample was determined in accordance with (ASTM D4373 2021) using a rapid carbonate analyzer (HM-4501, Humboldt). Calibration was performed with 99.9% pure ACS grade calcium carbonate. 1 N hydrochloric acid was used for dissolving the carbonates, and the pressure exerted by CO_2 was taken after a reaction time of 10 minutes.

RESULTS AND DISCUSSION

Evidence of Microbial Life in Fly Ash During MICP Treatment.

The presence of microbial cells observed during the MICP treatment (Figure 2) shows that microbial life was indeed possible in fly ash despite the theoretical pore size limitations of fly ash (Mitchell and Santamarina 2005), and the bacterial community was successfully stimulated during MICP treatment. This was due to the lightweight nature of fly ash and low realizable densities (0.8 g/cc in the present study) which resulted in a loose packing of fly ash particles and, hence effectively greater pore space compared to theoretical packing of spherical particles, thereby allowing for the growth of bacterial cells and development of microbial community during the MICP process. Studies in literature have also observed the presence of other microbial life forms such as diatoms (unicellular organisms of the algal class *Bacillariophycea*) in long-term ponded ash samples and its impact on hydraulic conductivity and dewatering of ash ponds in field conditions (Wirth et al. 2022). Hence, possibility of biological activity and its impacts in such low-density materials should be given due consideration and cannot be ignored.

The bacterial cell attachment and association with fly ash particles (Figure 2) showed that some of the bacterial cells were as large as the smallest fly ash spheres, indicating that bacterial cells need a certain minimum surface area for attachment, at least fly ash spheres of ~3.5 µm in diameter. Bacterial cell growth and division were also a function of fly ash particle size as the surface area of a fly ash sphere would become a limiting factor for further cell division (observe single cells on small ~3.5 µm spheres in Figure 2c compared to cluster of 7 cells on ~10 µm sphere in Figure 2a). However, the precipitated calcite during cementation treatments resulted in the bonding of different fly ash particles, which allowed for the growth and connection of bacterial cells across neighboring fly ash particles (Figure 2(c-f)).

Precipitated Calcite Profile.

The precipitated calcite profile of fly ash showed high zones of calcite near the inlet and outlet ports of the column (Figure 3). The high calcite precipitation observed near the inlet (bottom of column) could be due to the reactive transport developed due to low flow rate (4 mL/min) adopted for fly ash owing to its low hydraulic conductivity. This is in contrast to 15 mL/min for Ottawa F-110 sand column which did not show such calcite precipitation pattern. The flow rate of 4 mL/min was low enough for bacterial cells to initiate urea hydrolysis as the cementation treatments were injected through the fly ash column resulting in an increase in pH and

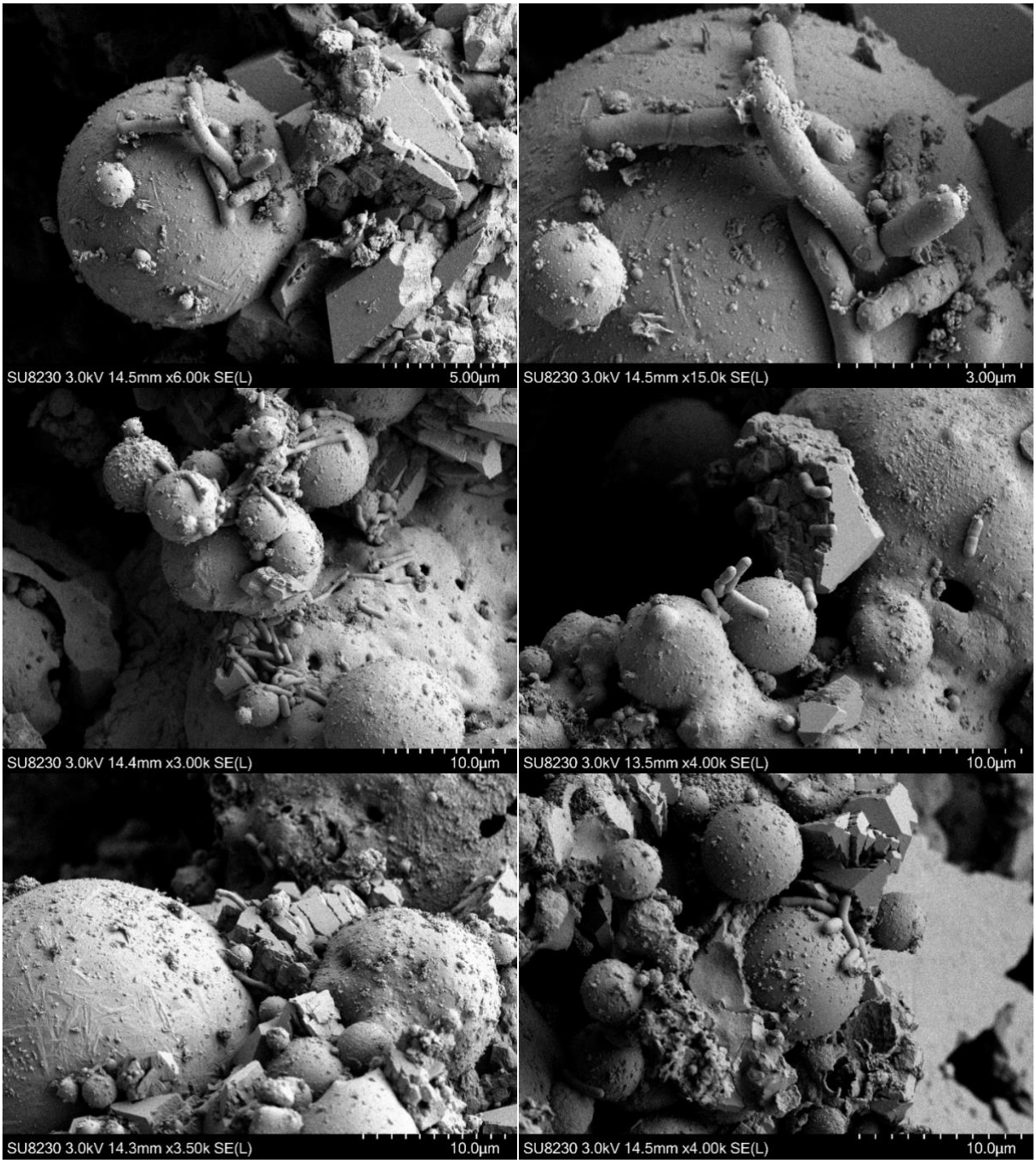

Figure 2. SEM images showing the presence of bacterial cells evidenced on bio-cemented fly ash particles at the end of MICP treatment.

simultaneous precipitation of calcite, thereby causing reactive transport. The high zone of calcite near the outlet (top of the column) was due to excess pore fluid standing on top of the fly ash material which resulted in the formation of a calcite layer (a crust layer was observed upon demolding of the column). This occurred due to the flushing of fine particles during the stimulation treatments and subsequent settling of fly ash particles through the column, upon cementation during the cementation phase of MICP.

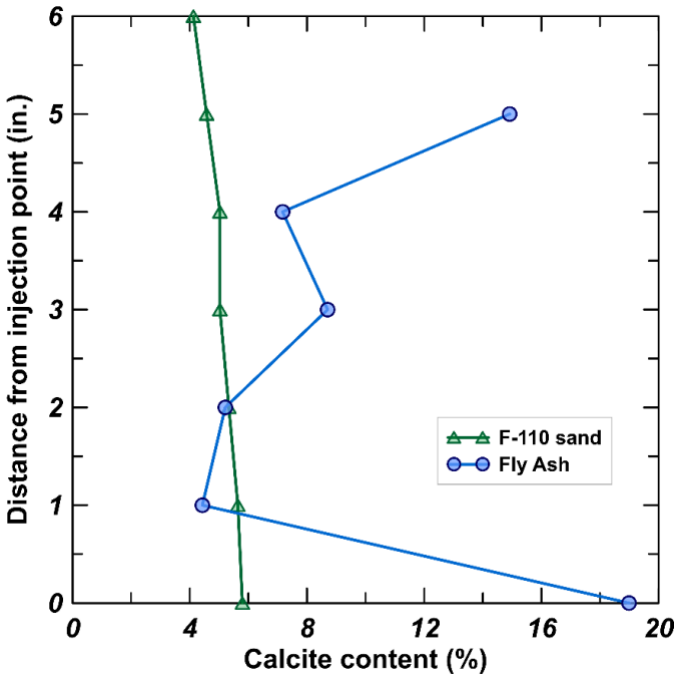

Figure 3. Comparison of precipitated calcite profile of MICP treated fly ash against benchmark Ottawa F-110 sand.

Another consideration for high calcite precipitation observed was the chemistry of fly ash, particularly its calcium oxide content which was ~6% (Wirth et al. 2019b). It is possible that the dissolution of calcium oxide during MICP treatment could mobilize Ca^{2+} ions which could then reprecipitate as calcite crystals, resulting in higher observed calcite contents. Furthermore, similar levels of calcite precipitation have been reported by Safavizadeh et al. (2019) in their MICP coal ash column experiments (~17.2% at bottom, ~8.8% in the middle, and ~3.2% at the top of the column), in which a flow rate of 7 mL/min and cementation recipe of 4:1, urea: $CaCl_2$, were adopted.

Fly Ash – Calcite Cementation Matrix.

The cementation pattern in fly ash was markedly different, with the fly ash particles embedded in a cementation matrix formed by precipitated calcite (Figure 4) compared to particle-to-particle cementation bonds observed in sands (DeJong et al. 2014; Al Qabany et al. 2012). The calcite crystal growth could have started on relatively larger fly ash particles or nucleated in the

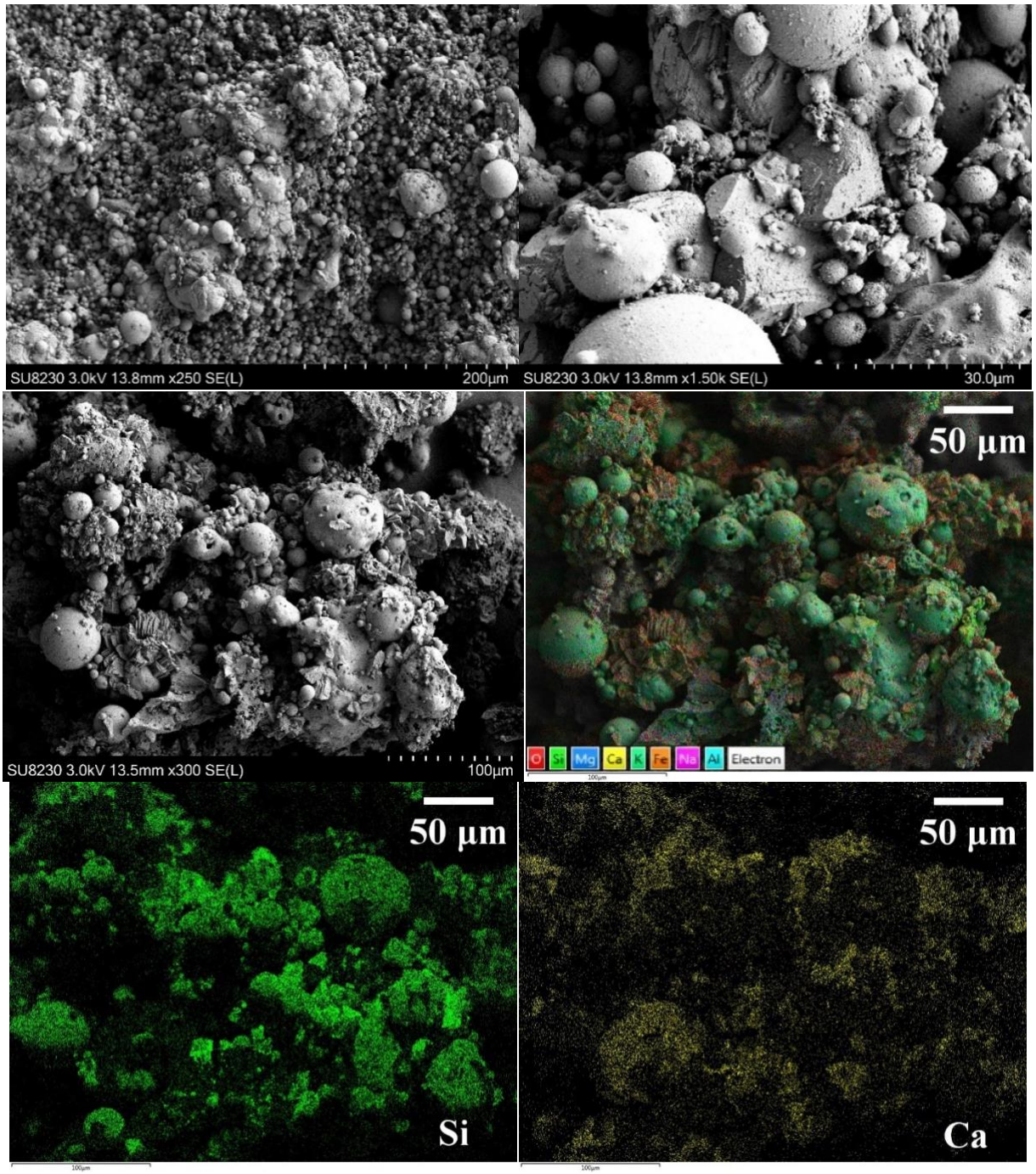

Figure 4. (A-C) Cemented block of fly ash particles and a magnified images showing the calcite bonds and bacteria. (D-F) SEM-EDS of image in (C) silicon (E) and calcium (F) maps showing the distribution of precipitated calcite and fly ash particles in a cemented block.

pore fluid solution, since the fly ash column was of low density, and progressively grew larger with every cementation treatment engulfing more fly ash particles. SEM-EDS of a cemented block of fly ash particles (Figure 4(c-f)) clearly showed the presence of calcium (Figure 4f) in the background underlying the fly ash particles (shown in green, Figure 4e), thus indicating that calcite

crystals were functioning as a cementation matrix in addition to forming cementation bonds between particles. The precipitated calcite crystals can individually grow to a size of ~5-20 µm which is in the range of D_{20} – D_{50} of untreated fly ash (Figure 5), i.e., the calcite crystals can grow to a size as large as fly ash particles of size D_{50}. Hence, smaller (<20 µm) fly ash particles are less likely to support calcite crystal growth on them, as is typically observed on sands, and therefore agglomeration starts to take place.

Agglomeration of Cemented Fly Ash Particles.

The D_{50} of MICP treated fly ash increased from 23.4 to 53.3 µm (Table 2), and a noticeable increase in particle size distribution of MICP treated fly ash sample (closest to injection point) can be observed from Figure 5. Cemented samples obtained from different depths were also tested, but the maximum increase in particle size was noticed for sample closest to the injection point (Table 2). During laser particle size analysis, the samples were dispersed using a stirrer at 3000 rpm along with ultrasonication resulting in the break-up of aggregations unless the particles were strongly bonded, which may have been the case of cemented fly ash sample closest to injection point, while the other samples could have undergone dispersion and de-aggregation.

Table 2. Comparison of D_{10}, D_{50}, and D_{90} between Untreated and MICP Treated Ash Samples

Particle size	Untreated fly ash sample	MICP treated ash samples Distance from injection point					
		0 (in.)	1 (in.)	2 (in.)	3 (in.)	4 (in.)	5 (in.)
d_{10}	**2.75 µm**	**5.41 µm**	2.77 µm	3.12 µm	2.82 µm	2.52 µm	2.73 µm
d_{50}	**23.4 µm**	**53.3 µm**	28.3 µm	33.4 µm	31.5 µm	25.7 µm	27.0 µm
d_{90}	**75.0 µm**	**164 µm**	101 µm	110 µm	103 µm	96.1 µm	99.6 µm

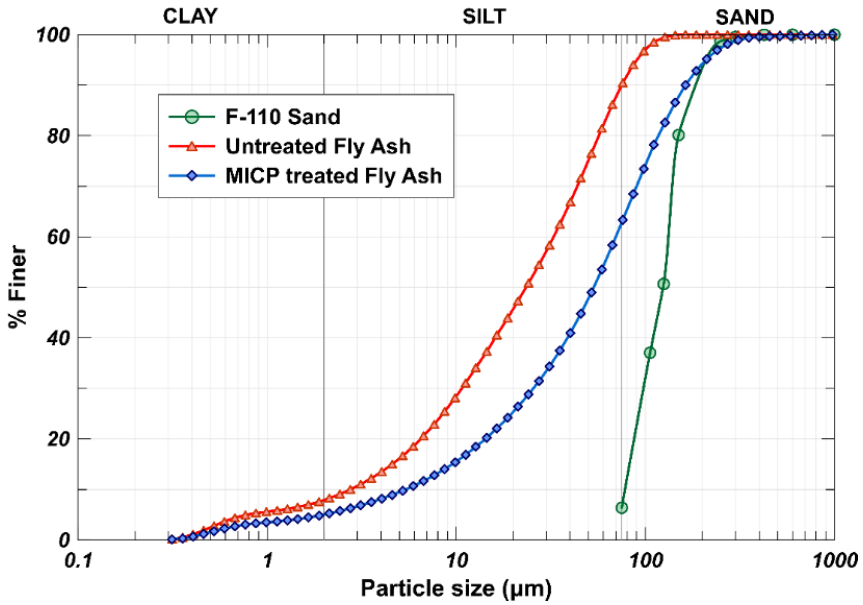

Figure 5. Particle size distribution of untreated fly ash sample and MICP treated fly ash sample (closest to injection point), obtained from Laser Particle Size Analyzer.

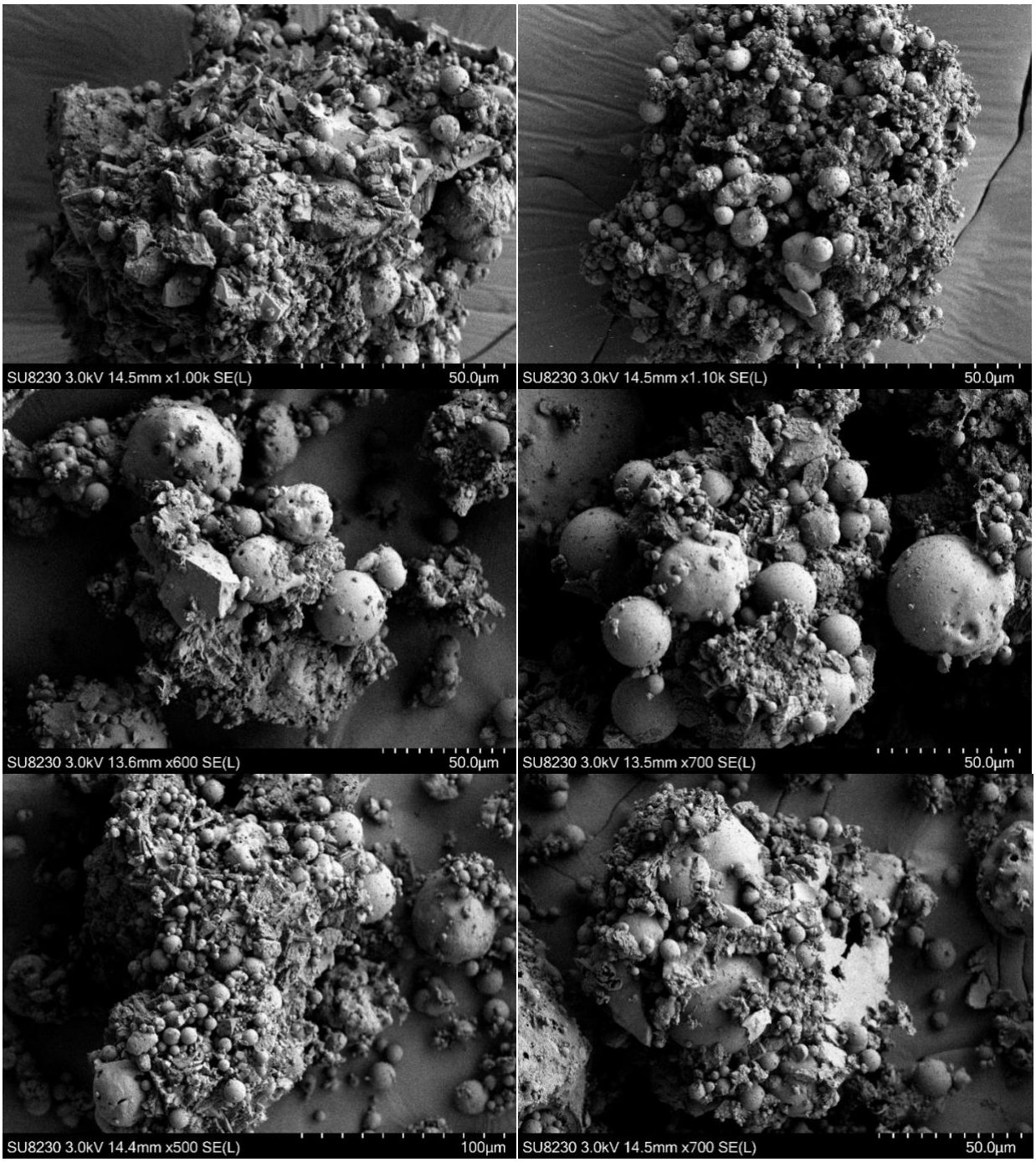

Figure 6. Agglomerated units of bio-cemented fly ash particles.

Aggregations of cemented fly ash particles were observed during SEM analysis (Figure 6) and were ~50 µm in size which agreed well with the laser particle size measurements. The inclusion of fly ash spheres and other aluminosilicates in the calcite matrix can be observed, suggesting that MICP treatment has the potential to aggregate fly ash particles into cemented units of larger sizes.

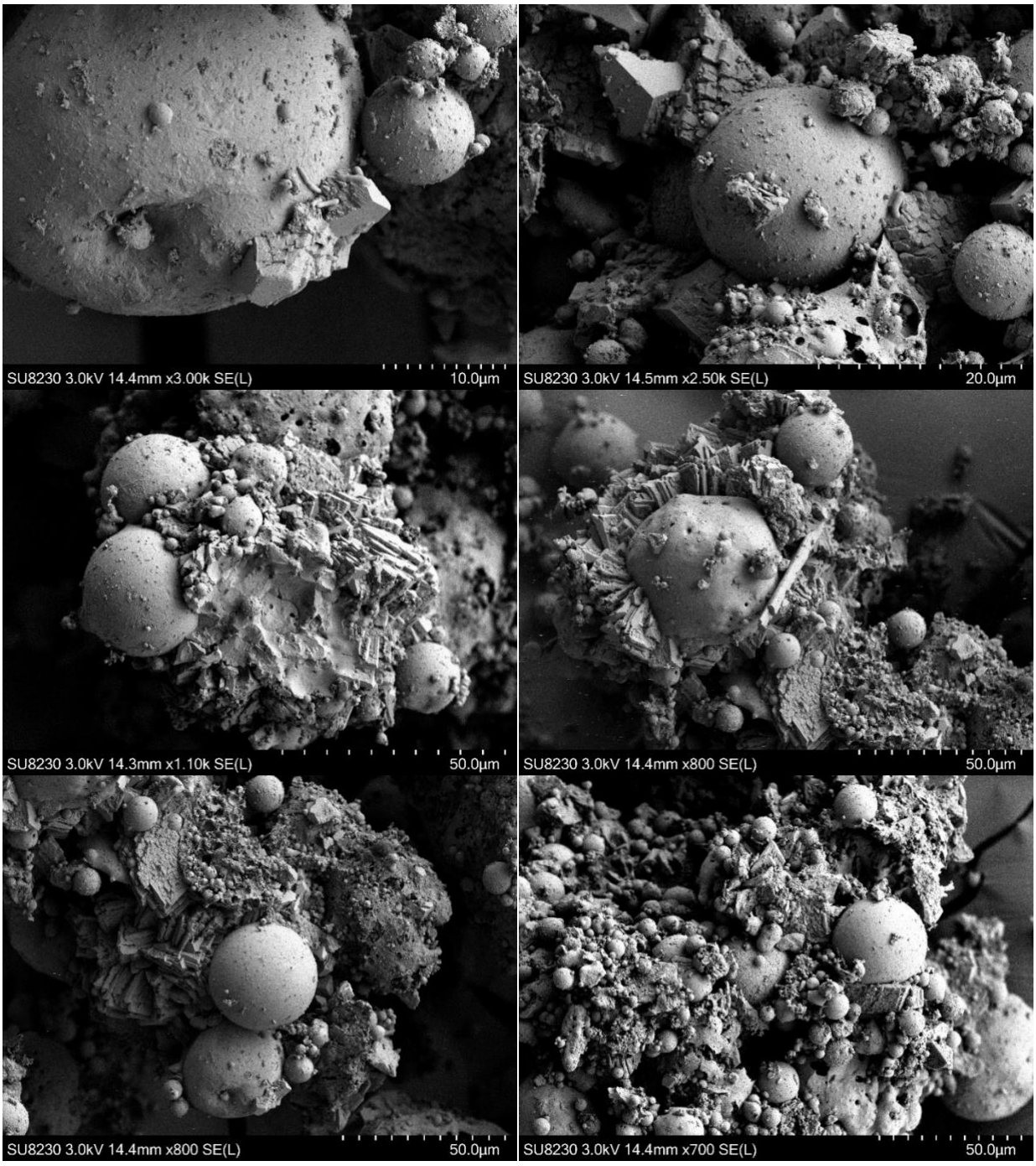

Figure 7. Effect of fly ash particle shape and size on calcite growth and cementation bonds.

Role of Fly Ash Morphology on Calcite Growth and Cementation Bonds.

The spherical particle shape of fly ash provides an opportunity to evaluate the role of particle shape on the nature of cementation bonds developed during MICP process, as spherical shape is a commonly used idealization in modelling in literature. The spherical shape of fly ash particles resulted in the formation of concave shaped calcite crystals (Figure 7(a and b)) as opposed to rhombohedral, trigonal face, and pyramidal-like morphologies of calcite crystals observed on sands. The resulting crystal growth was radially outward (Figure 7(b and d)), and furthermore,

the extent of crystal growth was also dependent on the size of the fly ash spheres. For a given calcite content, the cementation bonds formed between spheres would cover the highest area and would be more efficient compared to bonds between rounded/sub-rounded sand particles, as a sphere has lowest the surface area for a given volume, and the nature of this bonding between spherical particles can be observed from Figure 7(c-f).

CONCLUSION

The present study was undertaken to investigate the MICP process in fly ash, a relatively low-density material, and to provide microscopic insights into MICP treated fly ash. MICP column experiments were performed on an unweathered fly ash sample, and evidence of microbial life stimulated during MICP treatment were obtained from SEM analysis. Since fly ash is a low-density material, sufficient pore space was still available for the growth of microbial cells despite pore size constraints on microbial life. Microbial cell attachment and growth were found to be a function of surface area i.e., particle size of fly ash, and cementation of fly ash particles together resulted in higher surface area and higher chance for bacterial cells to interact, connect, and survive. Precipitated calcite contents in fly ash were much higher compared to benchmark Ottawa F-110 sand because of reactive transport due to low flow rate conditions. The precipitated calcite resulted in the formation of a cementation matrix in which fly ash particles were engulfed and embedded, which was a different mechanism compared to formation of cementation bonds or coating observed on sand particles. Furthermore, agglomeration of cemented fly ash particles into larger units of ~50 μm was observed, suggesting that MICP has the potential to aggregate fly ash particles. The spherical shape of fly ash resulted in concave shaped calcite bonds and radially outward crystal growth, while the size of fly ash spheres controlled the growth of calcite cementation matrix on and around their surfaces.

ACKNOWLEDGEMENTS

The authors are grateful to Dr. Nortey Yeboah and Southern Company for providing fly ash samples. This work was done as part of the Center-2-Center sub-project (PR75: C2C – ASU: Multi-scale Investigation of Bio-Based Mineral Precipitation in Carbonate Bearing Granular Soils and Construction Related Waste) of the Center for Bio-Inspired and Bio-Mediated Geotechnics (CBBG). This work was also performed in part at the Georgia Tech Institute for Electronics and Nanotechnology, a member of the National Nanotechnology Coordinated Infrastructure (NNCI), which is supported by the National Science Foundation (Grant ECCS-2025462).

REFERENCES

1. Achal, V., A. Mukherjee, and M. S. Reddy. 2011. “Microbial Concrete: Way to Enhance the Durability of Building Structures.” *Journal of Materials in Civil Engineering*, 23 (6): 730–734. https://doi.org/10.1061/(ASCE)MT.1943-5533.0000159.
2. Adams, T. H. 2022. “Coal Combustion Products Production and Use Reports.” American Coal Ash Association.

3. ASTM D4373. 2021. “Standard Test Method for Rapid Determination of Carbonate Content of Soils.” West Conshohocken, PA: ASTM International.

4. Black, A. P. 2015. “Production and Use of Coal Combustion Products in the US.” American Road and Transportation Builders Association.

5. Choi, S.-G., K. Wang, Z. Wen, and J. Chu. 2017. “Mortar crack repair using microbial induced calcite precipitation method.” *Cem Concr Compos*, 83: 209–221. https://doi.org/10.1016/j.cemconcomp.2017.07.013.

6. Chu, J., V. Stabnikov, and V. Ivanov. 2012. “Microbially Induced Calcium Carbonate Precipitation on Surface or in the Bulk of Soil.” *Geomicrobiol J*, 29 (6): 544–549. https://doi.org/10.1080/01490451.2011.592929.

7. Cuthbert, M. O., L. A. McMillan, S. Handley-Sidhu, Michael. S. Riley, D. J. Tobler, and Vernon. R. Phoenix. 2013. “A Field and Modeling Study of Fractured Rock Permeability Reduction Using Microbially Induced Calcite Precipitation.” *Environ Sci Technol*, 47 (23): 13637–13643. https://doi.org/10.1021/es402601g.

8. DeJong, J. T., M. G. Gomez, A. C. M. S. Pablo, C. M. R. Graddy, D. C. Nelson, M. Lee, K. Ziotopoulou, M. El Kortbawi, B. Montoya, and T.-H. Kwon. 2022. “State of the Art: MICP soil improvement and its application to liquefaction hazard mitigation.” *Proceedings of the 20th ICSMGE*, (1): 405–508.

9. DeJong, J. T., K. Soga, E. Kavazanjian, S. Burns, L. A. Van Paassen, A. Al Qabany, A. Aydilek, S. S. Bang, M. Burbank, L. F. Caslake, C. Y. Chen, X. Cheng, J. Chu, S. Ciurli, A. Esnault-Filet, S. Fauriel, N. Hamdan, T. Hata, Y. Inagaki, S. Jefferis, M. Kuo, L. Laloui, J. Larrahondo, D. A. C. Manning, B. Martinez, B. M. Montoya, D. C. Nelson, A. Palomino, P. Renforth, J. C. Santamarina, E. A. Seagren, B. Tanyu, M. Tsesarsky, and T. Weaver. 2014. “Biogeochemical processes and geotechnical applications: progress, opportunities and challenges.” *Bio- and Chemo-Mechanical Processes in Geotechnical Engineering*, 143–157. ICE Publishing.

10. Feng, J., B. Chen, W. Sun, and Y. Wang. 2021. “Microbial induced calcium carbonate precipitation study using Bacillus subtilis with application to self-healing concrete preparation and characterization.” *Constr Build Mater*, 280: 122460. https://doi.org/10.1016/j.conbuildmat.2021.122460.

11. Gomez, M. G., C. M. R. Graddy, J. T. DeJong, D. C. Nelson, and M. Tsesarsky. 2018. “Stimulation of Native Microorganisms for Biocementation in Samples Recovered from Field-Scale Treatment Depths.” *Journal of Geotechnical and Geoenvironmental Engineering*, 144 (1). https://doi.org/10.1061/(ASCE)GT.1943-5606.0001804.

12. Kang, C.-H., S.-H. Han, Y. Shin, S. J. Oh, and J.-S. So. 2014. “Bioremediation of Cd by Microbially Induced Calcite Precipitation.” *Appl Biochem Biotechnol*, 172 (6): 2907–2915. https://doi.org/10.1007/s12010-014-0737-1.

13. Lee, M., M. G. Gomez, A. C. M. San Pablo, C. M. Kolbus, C. M. R. Graddy, J. T. DeJong, and D. C. Nelson. 2019. “Investigating Ammonium By-product Removal for Ureolytic Bio-cementation Using Meter-scale Experiments.” *Sci Rep*, 9 (1): 18313. Springer US. https://doi.org/10.1038/s41598-019-54666-1.

14. Mitchell, J. K., and J. C. Santamarina. 2005. “Biological Considerations in Geotechnical Engineering.” *Journal of Geotechnical and Geoenvironmental Engineering*, 131 (10): 1222–1233. https://doi.org/10.1061/(asce)1090-0241(2005)131:10(1222).

15. Montoya, B. M., J. T. DeJong, and R. W. Boulanger. 2013. “Dynamic response of liquefiable sand improved by microbial-induced calcite precipitation.” *Bio- and Chemo- Mechanical Processes in Geotechnical Engineering - Geotechnique Symposium in Print 2013*, (4): 125–135. https://doi.org/10.1680/bcmpge.60531.012.

16. Montoya, B. M., S. Safavizadeh, and M. A. Gabr. 2019. “Enhancement of Coal Ash Compressibility Parameters Using Microbial-Induced Carbonate Precipitation.” *Journal of Geotechnical and Geoenvironmental Engineering*, 145 (5): 1–14. https://doi.org/10.1061/(asce)gt.1943-5606.0002036.

17. Phillips, A. J., A. B. Cunningham, R. Gerlach, R. Hiebert, C. Hwang, B. P. Lomans, J. Westrich, C. Mantilla, J. Kirksey, R. Esposito, and L. Spangler. 2016. “Fracture Sealing with Microbially-Induced Calcium Carbonate Precipitation: A Field Study.” *Environ Sci Technol*, 50 (7): 4111–4117. https://doi.org/10.1021/acs.est.5b05559.

18. Phillips, A. J., R. Gerlach, E. Lauchnor, A. C. Mitchell, A. B. Cunningham, and L. Spangler. 2013. “Engineered applications of ureolytic biomineralization: a review.” *Biofouling*, 29 (6): 715–733. https://doi.org/10.1080/08927014.2013.796550.

19. Al Qabany, A., K. Soga, and C. Santamarina. 2012. “Factors Affecting Efficiency of Microbially Induced Calcite Precipitation.” *Journal of Geotechnical and Geoenvironmental Engineering*, 138 (8): 992–1001. https://doi.org/10.1061/(ASCE)GT.1943-5606.0000666.

20. Safavizadeh, S., B. M. Montoya, and M. A. Gabr. 2019. “Microbial induced calcium carbonate precipitation in coal ash.” *Geotechnique*, 69 (8): 727–740. https://doi.org/10.1680/jgeot.18.P.062.

21. Wirth, X., D. Benkeser, N. N. N. Yeboah, C. R. Shearer, K. E. Kurtis, and S. E. Burns. 2019a. “Evaluation of Alternative Fly Ashes as Supplementary Cementitious Materials.” *ACI Mater J*, 116 (4): 69–77. American Concrete Institute. https://doi.org/10.14359/51716712.

22. Wirth, X., D. A. Glatstein, and S. E. Burns. 2019b. “Mineral phases and carbon content in weathered fly ashes.” *Fuel*, 236: 1567–1576. https://doi.org/10.1016/j.fuel.2018.09.106.

23. Wirth, X., S. M. Tyndale, S. H. Shivaprakash, and S. E. Burns. 2022. “Water Retention and Hydraulic Conductivity Characteristics of Ponded Fly Ash.” *Geo-Congress 2022*, 484–494. Reston, VA: American Society of Civil Engineers.